Scattering of gap solitons by $\mathcal{PT}$-symmetric defects

F. Kh. Abdullaev,[1,2] V. A. Brazhnyi,[3] and M. Salerno[4]

[1]*Physical - Technical Institute, Uzbek Academy of Sciences, 2-b, G. Mavlyanov str., 100084 Tashkent, Uzbekistan*

[2]*P Kulliyyah of Science, IIUM, Jalan Istana, Bandar Indera Mahkota, 25200 Kuantan, Pahang Darul Makmur, Malaysia*

[3]*Centro de Física do Porto, Faculdade de Ciências, Universidade do Porto, R. Campo Alegre 687, Porto 4169-007, Portugal*

[4]*Dipartimento di Fisica "E. R. Caianiello", Universitá di Salerno, via Giovanni Paolo II, stecca 9, I-84084 Fisciano (SA), Italy*

(Received 14 August 2013; published xxxxx)

The resonant scattering of gap solitons (GSs) of the periodic nonlinear Schrödinger equation, with a localized defect which is symmetric under the parity and the time-reversal ($\mathcal{PT}$) symmetry, is investigated. It is shown that for suitable amplitudes ratios of the real and imaginary parts of the defect potential the resonant transmission of the GS through the defect becomes possible. The resonances occur for potential parameters which allow the existence of localized defect modes with the same energy and norm of the incoming GS. Scattering properties of gap solitons of different band gaps with effective masses of opposite sign are investigated. The possibility of unidirectional transmission and blockage of gap solitons by $\mathcal{PT}$ defect, as well as, amplification and destruction induced by multiple reflections from two $\mathcal{PT}$ defects, are also discussed.

DOI: 10.1103/PhysRevA.00.003800 PACS number(s): 42.65.Tg, 03.75.Nt, 05.30.Jp

I. INTRODUCTION

Recently it has been shown that non-Hermitian Hamiltonians that are symmetric with respect to both parity and time-reversal ($\mathcal{PT}$) symmetry can have a fully real spectrum, in spite of the non-Hermiticity of the Hamiltonian [1]. This observation has attracted the attention of many researchers, both for theoretical developments of dissipative systems in quantum mechanics, and for developments of concrete applications in the fields of optics [2], plasmonics [3], electronics [4], and metamaterials [5].

In particular, in the field of nonlinear optics, $\mathcal{PT}$-symmetric potentials are presently investigated for management of light propagation in media with specific spatial distributions of gain and losses [2]. In this context, many interesting phenomena have been reported, including double refraction of beams [6], nonreciprocal propagation in periodic $\mathcal{PT}$-symmetric media [7], existence of optical solitons [8,9], routing in optical $\mathcal{PT}$-symmetric mesh lattices [10], etc. $\mathcal{PT}$-symmetric lattices have also been suggested for realizations in resonant media with three-level atoms [11].

The scattering of usual continuous and discrete solitons by localized $\mathcal{PT}$ potentials have been recently investigated in [12] for the case of Scarf II type $\mathcal{PT}$ potential, and in [13] for $\mathcal{PT}$ defects in a quasilinear regime where it has been shown that reflected and transmitted small amplitude waves can be amplified in the scattering process. The possibility of soliton switching in a $\mathcal{PT}$-symmetric coupler induced by the gain and loss properties of the $\mathcal{PT}$ defect was also suggested in [14].

Existence and stability of defect-gap solitons in real periodic optical lattices (OLs) with $\mathcal{PT}$-symmetric nonlinear potentials have been demonstrated in [15]. In this context, particular attention has been devoted to the scattering properties of linear waves propagating in $\mathcal{PT}$-symmetric optical media, as well as to the existence of localized states, both in linear and nonlinear cases. The existence and stability of gap solitons (GSs) in $\mathcal{PT}$-symmetric lattices with single-sided defects were considered in [16,17] for the continuous case, and for the discrete case with a nonlocal nonlinearity in [18], where it was shown that nonlocality can enlarge soliton existence regions in parameter space.

Scattering of GSs by localized defects has been extensively investigated in the conservative case. In particular, the existence of repeated reflection, transmission, and trapping regions for increasing defect amplitudes has been demonstrated in [19] where the phenomenon of resonant transmission was discussed and ascribed to the existence of defect modes matching the energy and the norm of the incoming GS. Moreover, it was shown that the number of resonances observed in the scattering coincides with the number of bound states existing inside the defect potential and that the sign of the effective mass of the GS plays an important role in the interaction with the defect potential [19]. Scattering properties of GSs by $\mathcal{PT}$-symmetric defect potentials, to the best of our knowledge, have not been investigated. Quite recently, the existence of defect modes of $\mathcal{PT}$-symmetric OLs has been experimentally reported in [20].

Possible extensions of the above conservative results to the case of $\mathcal{PT}$ defects can be of interest in several respects. In particular, it is interesting to see if the interpretation of the scattering properties in terms of resonances with $\mathcal{PT}$ defect modes is still valid. In addition, the interplay between effective mass, potential amplitudes, and interaction is also very interesting to explore in the presence of $\mathcal{PT}$-symmetric defects.

The aim of the present paper is to investigate the scattering properties of a GS of the periodic nonlinear Schrödinger equation (NLSE) by localized $\mathcal{PT}$-symmetric defects. In particular, we show that resonant transmissions of GSs through a $\mathcal{PT}$ defect become possible for amplitude ratios of real and imaginary parts of the $\mathcal{PT}$ potential which allow the existence of defect modes with the same energy and norm of the incoming GS. For $\mathcal{PT}$ defects with a small imaginary part, the scattering properties are found to be very similar to those reported for the conservative case [19]. As the imaginary part of the $\mathcal{PT}$ defect potential is increased, however, we show that GS can be strongly amplified or depleted especially when potential parameters are very close to higher resonance. Resonant transmission peaks obtained from direct numerical integrations of the NLS equation are found to be in all cases in good agreement with those predicted by a stationary $\mathcal{PT}$ defect mode analysis.

Scattering properties of GS with different effective masses are also investigated. In particular, we show that GS with opposite effective mass behave similarly when the sign of the $\mathcal{PT}$ defect is reversed, this confirms the validity of an effective mass description in the scattering by $\mathcal{PT}$ defects. The possibility of unidirectional transmission of GS through $\mathcal{PT}$ defects, and the amplification or destruction of a GS trapped between two $\mathcal{PT}$ defects, are also considered at the end. Finally, we remark that $\mathcal{PT}$-symmetric potentials are presently experimentally implemented in optical systems and we expect that the above results can have experimental implementations in systems similar to the one considered in [20].

The paper is organized as follows. In Sec. II we introduce the model equation and discuss the main properties of the system. In Sec. III we present scattering results obtained from direct numerical PDE integrations of the system, for resonant transmissions, trapping, and reflections of a GS through a $\mathcal{PT}$ defect, as a function of the potential parameters. This is done both for a GS of the semi-infinite gap and for GS of the first band gap, with positive and negative effective masses, respectively, and the results are compared with those obtained from defect mode analysis. In Sec. IV we discuss possible applications of the scattering properties of a GS both by a single $\mathcal{PT}$ defect and by a couple of defects, while in the last section the main results of the paper are briefly summarized.

II. THE MODEL

The model equation we consider is the following normalized one-dimensional NLSE:

$$i\Psi_t = -\Psi_{xx} + [V_{\mathrm{ol}}(x) + V_d(x)]\Psi + \sigma|\Psi|^2\Psi, \tag{1}$$

with $V_{\mathrm{ol}}(x)$ denoting a periodic potential (optical lattice) of period L $[V_{\mathrm{ol}}(x) = V_{\mathrm{ol}}(x+L)]$ and V_d is a localized $\mathcal{PT}$-symmetric complex defect introducing gain and loss in the system.

This equation arises in connection with the propagation of a plane light beam in a Kerr nonlinear media with a linear complex refraction index $n(x) = n_R(x) + in_I(x)$ introducing periodic modulation and localized gain-loss distribution in the transverse x-direction. As is well known, the wave equation for the propagation of the electric field of the beam, in the paraxial approximation, can be written as

$$iE_z + \frac{1}{2\beta}E_{xx} + k_0[n_R(x) + in_I(x) + \sigma|n_2||E|^2]E = 0, \tag{2}$$

where $E(x,z)$ is the electric field, z is the longitudinal (propagation) distance, $\beta = n_0k_0 = 2\pi n_0/\lambda_0$ is the propagation constant, with n_0 and n_2 as the background and quadratic parts of the refraction index, respectively, and with σ fixing the sign of the coefficient of the Kerr nonlinearity (e.g., $\sigma = 1$ for focusing and $\sigma = -1$ for defocusing cases). It is known that in order to satisfy the $\mathcal{PT}$ symmetry $n_R(x)$ must be an even function while the gain-loss component $n_I(x)$ must be odd. Equation (1) then follows from Eq. (2) after introducing dimensionless variables $t = \frac{z}{L_b}, x = \frac{x}{x_b}$ and the rescaling of the field amplitude and refraction index according to

$$\sqrt{k_0|n_2|L_b}\;E = \Psi, \quad 2\beta^2x_b^2n(x) = V_{\mathrm{ol}} + V_d \tag{3}$$

(here x_b denotes the initial width of the beam and $L_b = \beta x_b^2$ is its diffraction length). In the following we fix $V_{\mathrm{ol}} = V_0\cos(2x)$ and take the defect potential $V_d(x)$ of the form

$$V_d(x) = \frac{\eta + i\xi x}{\sqrt{2\pi}\,\Delta}\exp[-(x-x_0)^2/(2\Delta^2)], \tag{4}$$

where η is the strength of the conservative part of the defect while coefficient ξ stands for the gain-dissipation parameter. The width of the defect is fixed to $\Delta = 5$ in all numerical calculations. Similar $\mathcal{PT}$ defect was also considered recently in Ref. [17]. Although in this paper we mainly concentrate on the case of a single $\mathcal{PT}$ defect, some result about the scattering of GSs from two $\mathcal{PT}$ defects will also be discussed at the end.

As it is well known, in the absence of any defect potential, Eq. (1) possesses families of exact GS solutions with energy (propagation constant) located in the band gaps of the linear eigenvalue problem

$$\frac{d^2\varphi_{\alpha k}}{dx^2} + [E_\alpha(k) - V_{\mathrm{ol}}(x)]\varphi_{\alpha k} = 0, \tag{5}$$

where $\varphi_{\alpha k}(x)$ are an orthonormal set of Bloch functions with α denoting the band index and k is the crystal momentum inside the first Brillouin zone (BZ): $k \in [-1,1]$. It is also known that small-amplitude GSs with energies E_s very close to band edges are of the form $\psi(x,t) = A(\zeta,\tau)\varphi_{\alpha k}(x)e^{-iE_\alpha(k)t}$ with the envelope function $A(\zeta,\tau)$ obeying the following NLSE:

$$i\frac{\partial A}{\partial\tau} = -\frac{1}{2M_{\mathrm{eff}}}\frac{\partial^2 A}{\partial\zeta^2} + \chi|A|^2A, \tag{6}$$

where τ and ζ are slow temporal and spatial variables, $M_{\mathrm{eff}} = (d^2E_\alpha/dk^2)^{-1}$ denotes the soliton effective mass, and $\chi = \sigma\int|\varphi_{\alpha k}|^4dx$ is the effective nonlinearity [22]. The condition for the existence of such solitons is $\chi M_{\mathrm{eff}} < 0$ [21] and coincides with the condition for the modulational instability of Bloch wave functions at the edges of the BZ [22]. In the presence of an OL with a localized $\mathcal{PT}$ defect, the linear spectral problem will still display a band structure but with additional localized states (defect modes) that are associated with real eigenvalues (in band gaps) when the imaginary part of the potential is below a critical value $|\xi_c| = |\eta|/\sqrt{2}\Delta$. Above this point, defect mode spectrum becomes mixed with complex pairs of eigenvalues, this corresponding to a dynamical breaking of the $\mathcal{PT}$ symmetry [23]. We remark that in nonlinear optics, $\mathcal{PT}$ symmetry and $\mathcal{PT}$-symmetry breaking have been both observed experimentally [24,25].

III. SCATTERING OF GS BY A $\mathcal{PT}$ DEFECT: NUMERICAL RESULTS

In order to investigate scattering properties of a GS by a localized $\mathcal{PT}$ defect, we compute by means of direct numerical integrations of Eq. (1) the transmission (T), trapping (C), and reflection (R) coefficients defined as

$$\begin{aligned} T &= \frac{1}{N_0}\int_{x_c}^{\infty}|\Psi(x,t_s)|^2dx, \\ C &= \frac{1}{N_0}\int_{-x_c}^{x_c}|\Psi(x,t_s)|^2dx, \\ R &= \frac{1}{N_0}\int_{-\infty}^{-x_c}|\Psi(x,t_s)|^2dx, \end{aligned} \tag{7}$$

where the integrals are evaluated after a sufficient long time t_s (typically $t_s \approx 20\,000$), for the process to become stationary. Here N_0 denotes the initial norm of the incoming GS [e.g., $\int_{-\infty}^{\infty} |\Psi(x,t=0)|^2 dx$], and the interval $[-x_c, x_c]$ represents the trapping region around the $\mathcal{PT}$ defect, with x_c fixed in all our calculations to $x_c = 30L$. In particular, we are interested in characterizing the dependence of the above coefficients on the $\mathcal{PT}$ defect parameters η and ξ, both for a GS of the semi-infinite gap and for a GS of the first band gap, having positive and negative effective masses, respectively. Notice that different from the conservative case, the sum of the above coefficients is not normalized to 1, e.g., $R + T + C \neq 1$, due to the presence of gain and loss in the system which does not allow the norm conservation. In particular, the above coefficients during the scattering can become larger than one due to the gain action of the $\mathcal{PT}$ defect. In all numerical investigations reported below, the GS is constructed as a stationary solution of the periodic NLS equation located at a large distance ($\approx 100L$) from the $\mathcal{PT}$ defect (far away from the defect such states practically coincide with of the NLSE with a perfect OL). The stationary GS is then put in motion by means of the phase imprinting technique, e.g., by applying a linear phase $e^{-i\sigma v x/2}$ to the stationary wave function.

A. GS of the semi-infinite gap

Let us first consider the case of a GS of the semi-infinite gap, e.g., with $\sigma = -1$ in Eq. (1), with energy (propagation constant) $E_s = -0.125$ close to the bottom edge of the lowest energy band. Initial GS profile and $\mathcal{PT}$ defect shape $V_d(x)$ are shown in Fig. 1 for the case $\xi = \pm 0.02|\eta|$. In the numerical experiment we apply an initial velocity to the GS, typically in the range 0.02–0.1, and gradually decreasing the strength of the defect parameter η under condition $\xi = \pm 0.02|\eta|$, in order to obtain the RCT coefficients depicted in Figs. 2(a) and 2(b) (see also Figs. 3, 4, 6, 9, 10 for the other cases discussed below). We see that for weak defect amplitudes and for the same GS initial velocity ($v = 0.05$), the positions of the T peaks, labeled B, C, and D in Fig. 2(a), mostly coincide with the ones of the conservative case considered in [19] (see Fig. 3 in [19]).

It is worth noting the differences in the behavior of the reflection coefficient. While in the case ($\xi = 0$) the coefficient R approaches the value 1 in the regions of nonexistence of defect modes, one can see that in the case $\xi = 0.02|\eta|$ the R coefficient in the interval $\eta \in [-6,0]$ in the total reflection regions becomes slightly greater than 1 [see Fig. 2(a)], meaning that during reflection the GS has been amplified by the defect. The opposite behavior is observed for the case $\xi = -0.02|\eta|$ [corresponding to the defect $\overline{V_d}(x)$], e.g., in the reflection regions inside the interval $\eta \in [-6,0]$ the reflection coefficient is always smaller than 1, meaning that the GS has been damped during the reflection [see Fig. 2(b)].

This behavior of the R coefficient may at a first sight appear counterintuitive, especially if one observes that in our numerical experiments the GS is always coming from the left and when it gets amplified (depleted) it arrives first at the loss (gain) side of the defect, from which one could expect just the opposite, e.g., a depletion (amplification) of the GS from the defect. The observed behavior, however, can be understood if one considers in more detail the GS dynamics during reflection. From an intuitive point of view one can argue that since for $\xi > 0$ ($\xi < 0$) the GS interacts first with the loss (gain), it passes this region with some velocity so that the turning point of its dynamics occurs more closely to the gain (loss) region

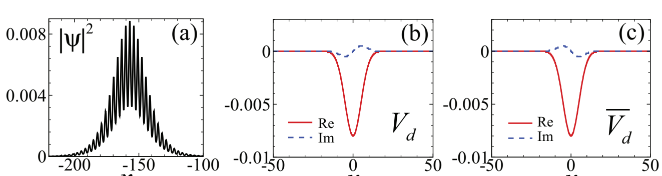

FIG. 1. (Color online) Initial profile of a GS located in the semi-infinite gap at (a) $E_s = -0.125$ and defect potential $V_d(x)$ with (b) $\xi = 0.02|\eta|$ and with (c) $\xi = -0.02|\eta|$. Other parameters are $\eta = -0.1$, $V_0 = -1$.

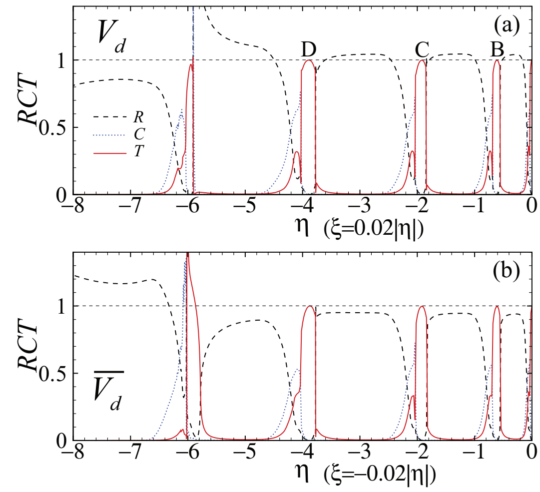

FIG. 2. (Color online) RCT diagram for (a) $V_d(x)$ with $\xi = 0.02|\eta|$ and (b) $\overline{V_d}(x)$ with $\xi = -0.02|\eta|$. Other parameters: $v = 0.05$, $E_s = -0.125$, $V_0 = -1$.

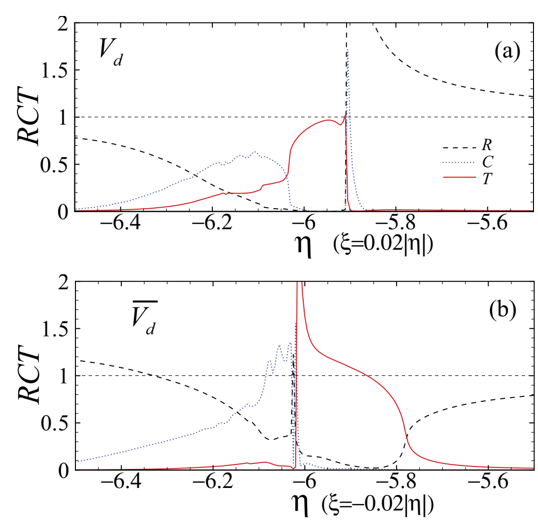

FIG. 3. (Color online) Zoom of Figs. 2(a) and 2(b) showing details in the interval $\eta \in [-6.5, -5.5]$ around the resonance.

of the defect (this is particularly true if the initial velocity is high or the imaginary part of the defect is small). Considering that the GS is an extended object and for the cases considered in this paper its typical width is of about $30L$ (see Fig. 1), e.g., much larger than the size of the defect with a width $\approx 8L$, this means that during the reflection the GS will be in any case exposed to the action of the gain (loss) side of the defect and the influence of this region on the dynamics will be larger as the closest will be the turning point at the origin. To understand if the GS will emerge amplified or depleted from the reflection it is convenient to consider the mean imaginary part of the defect potential seen by the GS at a given time defined as

$$\langle V_i \rangle(t) = \frac{1}{N_0} \int_{-\infty}^{\infty} \mathrm{Im}[V_d(x)] |\Psi(x,t)|^2 dx. \tag{8}$$

It is clear that if $\int \langle V_i \rangle dt$ is positive (negative), the amplification (depletion) of the GS is expected during the reflection.

This is exactly what it is shown in the right panels of Fig. 5, where results of two distinctive cases from Fig. 4, with $\eta = -5$ and $\eta = -7$, are reported. In the left panels of Fig. 5 we have depicted the trajectory of the center X,

$$X(t) = \frac{1}{N_0} \int x |\Psi(x,t)|^2 dx \tag{9}$$

of the density distribution during the reflection. One can see from this figure that, in agreement with our intuitive argument, for smaller values of $|\eta|$ (e.g., on the right side of resonance at $\eta \approx -6$) the GS can penetrate the defect more and in the cases in which the GS is amplified, the turning point of the trajectory always occurs closer (less close) to the origin for $\xi > 0$ ($\xi < 0$). The opposite behavior is observed for a GS that is depleted during the reflection.

Interesting results are also observed when the imaginary part of the defect potential is increased and the non-Hermitian character of the interaction contributes more significantly to the scattering. For the chosen ratio $\xi/|\eta| = 0.02$, this occurs around the value $\eta \leqslant -6$ as one can see from the details depicted in Fig. 3(a). From this it is clear that the interaction

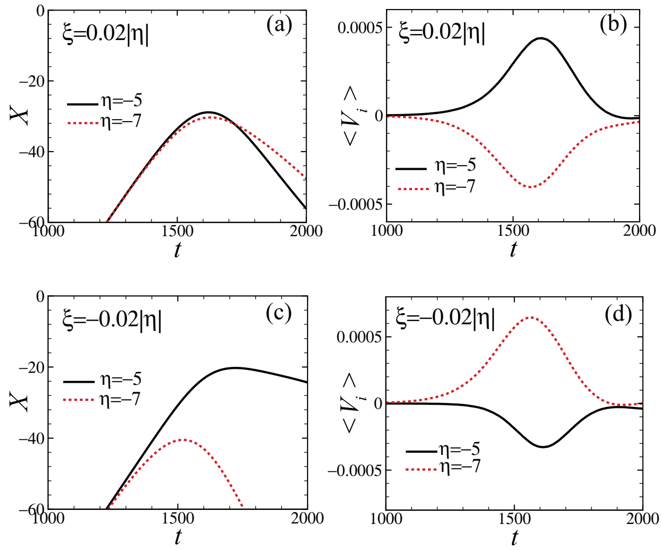

FIG. 5. (Color online) Trajectories of the center of the density distribution $X(t)$ in (a), (c) and mean imaginary part of $\mathcal{PT}$ defect $\langle V_i \rangle$ in (b), (d) of a GS during reflection. The top row panels (a), (b) corresponds to case $\xi = 0.02|\eta|$ and the bottom row panels (c), (d) to case $\xi = -0.02|\eta|$. Incoming GS velocity and other parameters are fixed as in Fig. 4.

of the GS with the loss and gain parts of the $\mathcal{PT}$ defect changes character when passing through the resonance point. In particular, one can see that near $\eta = -5.9$ the reflection coefficient shows a rapid growth corresponding to a strong amplification during the reflection. The explanation of this follows from the same arguments given above and from the fact that the interaction with almost resonant stationary defect modes will further prolong the interaction time that the GS has with the gain side of the defect, this results in a higher amplification. This effect can also be observed at lower resonances by decreasing the incoming GS velocity, as one can see from Fig. 6 for the rapid growth of T and R coefficients occurring around $\eta = -4$.

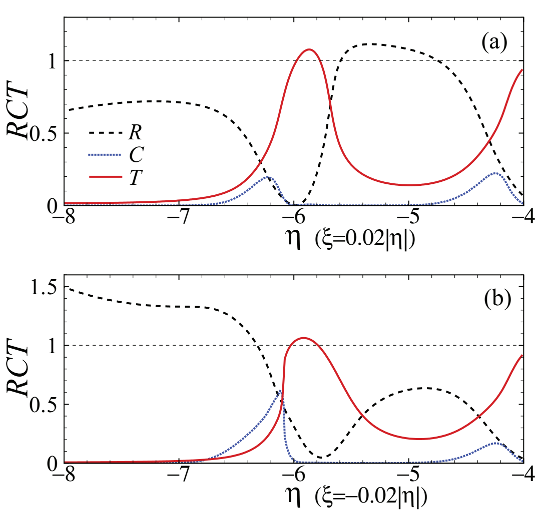

FIG. 4. (Color online) The same as in Fig. 3 but for an incoming GS velocity $v = 0.1$. Other parameters are fixed as in Figs. 2(a) and 2(b).

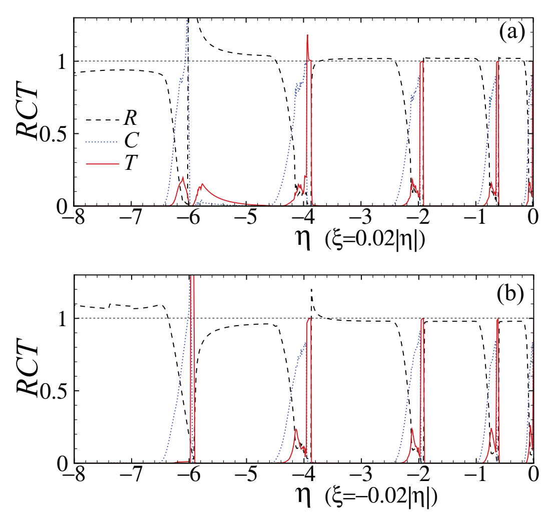

FIG. 6. (Color online) RCT diagram for (a) $\xi = 0.02|\eta|$ and (b) $\xi = -0.02|\eta|$. Other parameters: $v = 0.02$, $E_s = -0.125$, $V_0 = -1$.

From Figs. 2(a) and 2(b) it is also quite evident that the crossover of the R coefficient from $R > 1$ ($R < 1$) to $R < 1$ ($R > 1$) occurs for the case $\xi = 0.02|\eta|$ ($\xi = -0.02|\eta|$) when $|\eta|$ is increased through the resonant point $\eta = -6$. This change of behavior can be understood from the fact that by further increasing the imaginary part of the $\mathcal{PT}$ defect (as is the case when $|\eta| > 6$), one reaches the point in which the turning point of the GS dynamics will always occur in the defect side from where the soliton arrives, so that it is always depleted by V_d and amplified by $\overline{V}_d$. This explanation also correlates with the above arguments in terms of turning points and mean effective potentials $\langle V_i \rangle$.

From the more detailed Fig. 3, it appears evident that just beyond the point $\eta = -6$, trapping becomes dominant and due to strong interaction with defect modes, the GS becomes very unstable, leading to the irregular oscillatory behavior observed for the trapping coefficient in Fig. 3(b). By decreasing the velocity of the incoming GS, however, the transmission peaks become narrow (see Fig. 6) and the R coefficient becomes closer to 1 in the total reflection regions (scattering is less affected by the complex potential). This is a consequence of the fact that for a smaller velocity a small amount of the GS wave function penetrates the defect and the interaction with the complex part of the potential is reduced.

It is also interesting to discuss the case $\eta > 0$ for which the real part of the $\mathcal{PT}$ defect corresponds to a barrier potential rather than a potential well. This obviously does not allow the formation of any stationary mode inside the defect since in this case $C = 0$ and only transmissions or reflections of the GS are possible. For a conservative defect (e.g., for $\xi = 0$) it was shown in [19] that for large defect amplitudes the incoming GS is always totally reflected (e.g., $R = 1$ and $T = C = 0$). For a $\mathcal{PT}$ defect with $\eta > 0$, we find that while the transmission and trapping coefficients continue to be zeros for large η, the reflection coefficient, in accordance to our previous discussion, depends on the sign of ξ (as well as on the ratio $\xi/|\eta|$) and can be smaller or larger than 1 (see Fig. 7) depending on whether the GS is interacting more with the dissipative or with the gain side of the defect, respectively.

B. GS of first band gap

Scattering properties of a GS belonging to the first band gap in the case of self-focusing Kerr nonlinearity [$\sigma = 1$ in Eq. (1)] are quite similar to the ones discussed above. In this case, however, it is possible to have GS with a negative effective

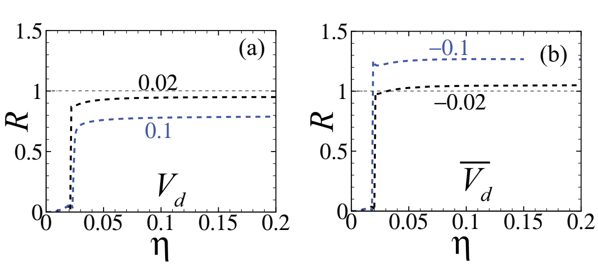

FIG. 7. (Color online) Behavior of the R coefficient in the scattering of a GS of the semi-infinite band gap with $v = 0.05$, by a $\mathcal{PT}$ defect with $\eta > 0$. The ratio $\xi/|\eta|$ is indicated near the corresponding curve.

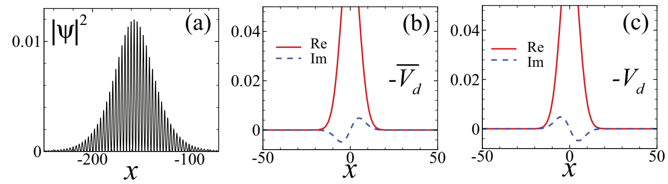

FIG. 8. (Color online) Initial profile of a GS located near the top of the lower band at (a) $E_s = 0.475$, and $\mathcal{PT}$ defect potential $V_d(x)$ for (b) $\xi = 0.02|\eta|$ and (c) $\xi = -0.02|\eta|$. Other parameters are $\eta = 1$, $V_0 = -1$.

mass if the Kerr nonlinearity is defocusing. To investigate the effects of a negative GS mass on the scattering properties we consider a GS of energy (propagation constant) $E_s = 0.475$ close to the top edge of the lowest band. The initial GS profile and shapes of defect potentials are depicted in Fig. 8. For parameters of the $\mathcal{PT}$ potential that are below the threshold of the spontaneous $\mathcal{PT}$-symmetry breaking (as is the case considered here) the spectrum is entirely real with a band structure that is only slightly affected by the defect. Since the effective mass is related to the curvature of the band we expect that an effective mass description of the GS dynamics should still be valid, at least for $\mathcal{PT}$ defects quite localized and with imaginary parts not too large. We remark here, however, that a proof of the validity of the effective mass theorem for periodic $\mathcal{PT}$ potentials is presently lacking (notice that in our case the OL is real and the $\mathcal{PT}$ symmetry is only coming from the defect). In an effective mass description one would expect that a change of sign in the effective mass can be compensated by a change of sign of the defect potential. If true, this would imply that the scattering properties of a GS with a positive effective mass by a $\mathcal{PT}$ defect potential V_d should be similar to those of a GS with negative effective mass scattered by a defect of opposite sign $-V_d$.

To check if this is true, we have applied an initial velocity to GS ($v = 0.05$) and constructed as in the previous cases the RCT coefficients as a function of the defect strength. The results are presented in Fig. 9 for the cases (a) $\xi/|\eta| = 0.02$ and (b) $\xi/|\eta| = -0.02$.

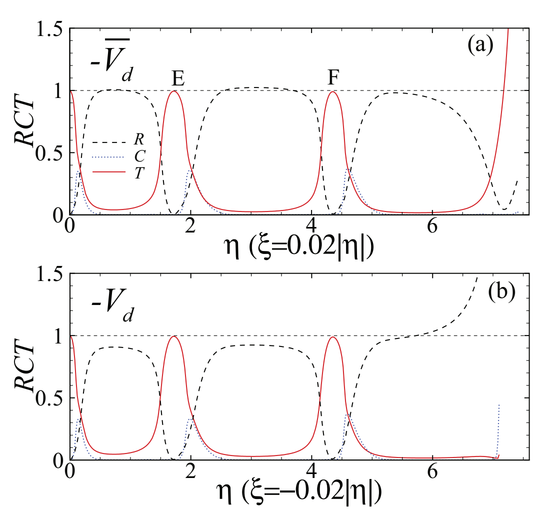

FIG. 9. (Color online) RCT diagram for (a) $\xi = 0.02\eta$ and (b) $\xi = -0.02\eta$. Other parameters: $v = 0.05$, $E_s = 0.475$, $V_0 = -1$.

By comparing the RCT diagram of the GS in a semi-infinite gap with defect V_d [see Fig. 2(a)] with the one in the first gap with defect $-V_d$ [see Fig. 9(b)], we see that, as expected, the scattering coefficients behave quite similarly in the two cases, except for the opposite behavior of the R coefficient at small values of $|\eta|$ (notice that R is slightly larger than 1 for the GS in the semi-infinite gap and smaller than 1 for the GS in the first gap). In particular, notice the rapid growth of the reflection coefficient R as one approaches the higher resonance in both cases. The discrepancy observed in the behavior of R for small values of $|\eta|$ can be ascribed to the different sizes of the GS in the two cases, as one can see from Figs. 1(a) and 8(a), respectively. The fact that the GS is wider in the first gap permits, for the same incoming velocity, a stronger interaction with the right side of the defect, than the one of the more localized GSs in the semi-infinite gap. Since the right side of the defect is of loss type for the GS in the first gap [see Fig. 8(c)] and of gain type for the GS in the semi-infinite gap [see Fig. 1(a)], this explains the observed discrepancy. Notice that this discrepancy is reduced by reducing the incoming GS velocity [compare Fig. 6(a) with Fig. 10(b)]. This can be understood from the reduction at small velocities of the interaction of the GS with the right side of the defect and from the smallness of η making the situation close to the one of the conservative case. Also notice that the decreasing of the incoming GS velocity (see Fig. 10) leads to the same effects discussed for GS from the semi-infinite gap (shrinking the transmission lines and approaching 1 of the R coefficient in the total reflection regions).

A similar situation is observed for the case $\xi = -0.02|\eta|$ (e.g., for potentials $\overline{V}_d$ and $-\overline{V}_d$) with the only difference that the discrepancy at small $|\eta|$ is now of opposite type and the rapid growth at the high resonance occurs for the T coefficient instead of R as one can see by comparing Fig. 2(b) with Fig. 9(a) [also compare Fig. 6(b) with Fig. 10(a) for the case of a smaller velocity].

We have also investigated the scattering properties of a negative mass GS by a $\mathcal{PT}$ defect with $\eta < 0$ (see Fig. 11). Notice, that due to the negative effective mass, the potential well corresponding to the real part of the $\mathcal{PT}$ defect will be seen by the GS as a potential barrier. This case should then be compared with the case $\eta > 0$ previously considered for the GS of the semi-infinite gap. Indeed, we find while transmission and trapping coefficients are zeros the reflection coefficient, in accordance to our previous discussion for a GS in the semi-infinite gap, depends on the sign of ξ and can be smaller or larger than 1 as one can see in Fig. 11. By comparing Fig. 11 with the corresponding Fig. 7, we see that a part of the discrepancy was discussed before and ascribed to the different sizes of the GS, the behavior is in qualitative good correspondence with what is expected from an effective mass description for two GSs of opposite effective masses.

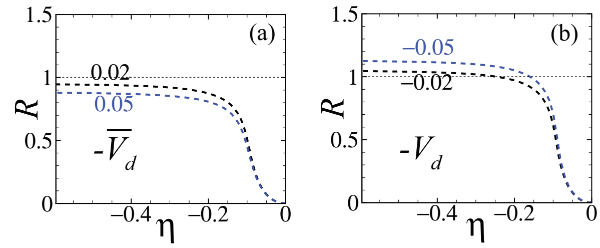

FIG. 11. (Color online) Behavior of the R coefficient for the scattering of a GS of the first band gap with negative effective mass $v = 0.05$ by a $\mathcal{PT}$ defect with $\eta < 0$. The ratio $\xi/|\eta|$ is indicated near the corresponding curve.

From the above results we conclude that GSs with opposite effective masses behave quite similarly in the presence of $\mathcal{PT}$ defect potentials of opposite signs, this being especially true for parameters values close to the high resonances.

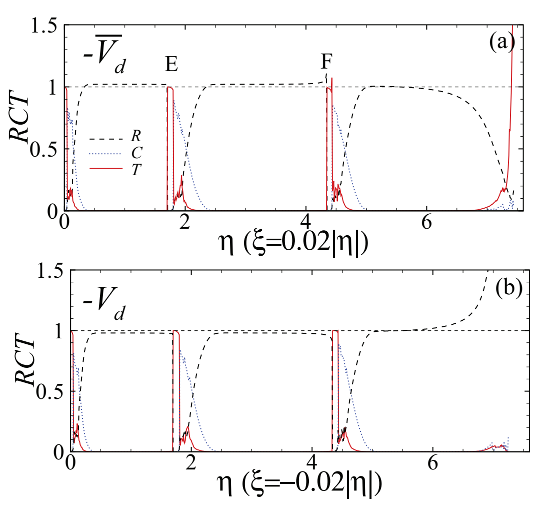

FIG. 10. (Color online) The same as in Fig. 9 but for a smaller incoming GS velocity $v = 0.02$. Other parameters are fixed as in Fig. 9.

C. Resonant transmission and $\mathcal{PT}$ defect mode analysis

To check the relevance of defect modes in the resonant transmission of a GS through a $\mathcal{PT}$ defect, we have explicitly calculated defect modes by solving the stationary eigenvalue problem associated with Eq. (1), and then compared results with those obtained by direct numerical integrations. This is reported in Fig. 12 from which we see that there is a good agreement between stationary defect mode analysis and dynamical calculations.

Second, we have checked that in all the considered cases the positions of the peaks observed in the RCT diagrams occur in correspondence with potential parameters that allow the existence of defect modes with the same energy and norm of the incoming GSs (see Figs. 13 and 14). In particular, in Fig. 13 we show the energy mismatch at the resonances between the GS and defect mode for two different cases, while in Fig. 14 we show, for corresponding cases, the behavior of the stationary and dynamical trapping coefficients as a function of η. We see from these figures that the agreement between mode analysis and numerical calculations is quite good both for the energy mismatch and for norms. In particular, notice that the positions of the peaks is in good agreement even for higher resonances where the imaginary part of the $\mathcal{PT}$ defect is not small, this confirms the validity of the defect modes interpretation for the resonant transmission of a GS through $\mathcal{PT}$ defects.

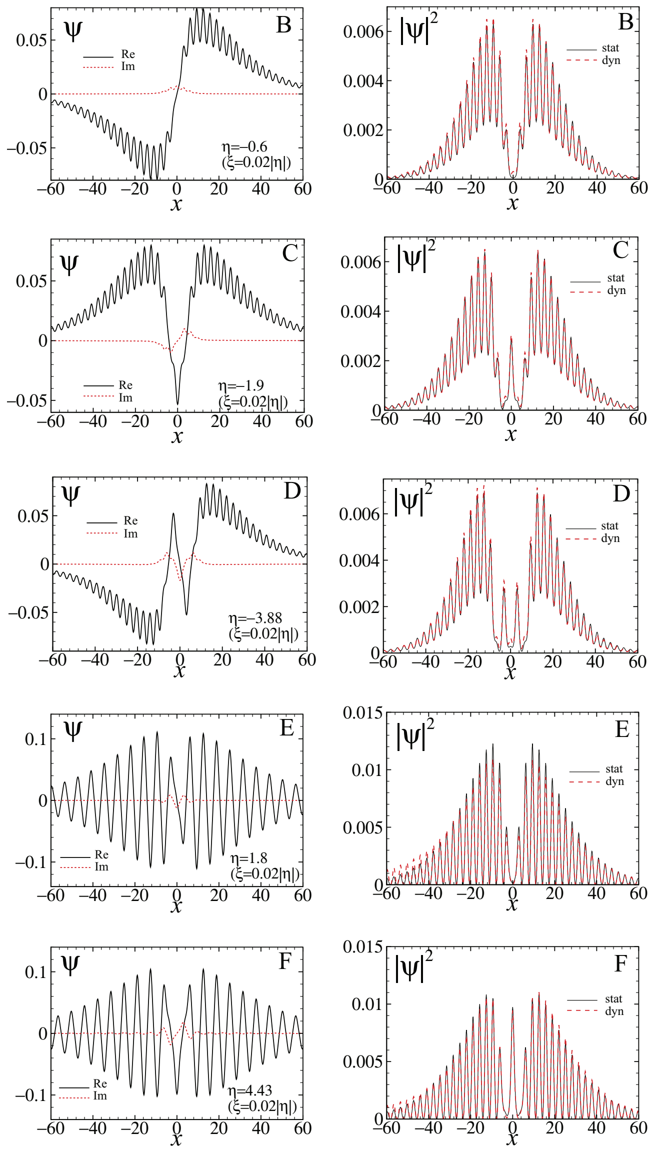

FIG. 12. (Color online) Top three rows: Stationary defect modes at the matching points B, C, and D of Fig. 2. Bottom two rows: Stationary defect modes at the matching points E and F of Fig. 9. In the left column the real (solid black) and imaginary (dashed red) parts of the defect mode are presented and in the right column its density (solid black) is compared to the defect mode calculated numerically (dashed red). In each row the defect modes at matching points are shown.

IV. MULTIPLE GS SCATTERING BY TWO $\mathcal{PT}$ DEFECTS

In this section we explore the nonreciprocity (spatial asymmetry) of the resonant transmission [26,27] that could be used for an unidirectional transmission/blockage of a GS through a $\mathcal{PT}$ defect (*diode effect*). For this we fix parameters of the defect potential in the region where it is possible to have total reflection (transmission) for the specific ratio value $\xi/|\eta| = 0.02$ (-0.02). Also we refer to the specific case of a GS located in the semi-infinite gap depicted in Fig. 15 (similar results can be obtained for GS of higher band gaps). For the above fixed ratio it is possible to observe asymmetric

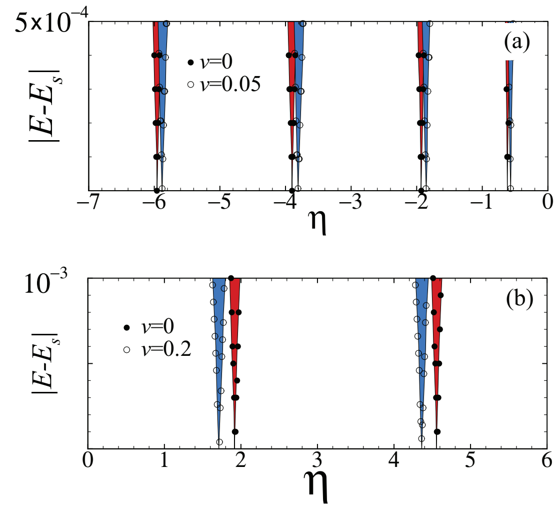

FIG. 13. (Color online) Energy mismatch $|E - E_s|$ between defect mode and incoming GS energies vs η, for $\xi/|\eta| = 0.02$, $E_s = -0.125$ (a) and $E_s = 0.475$ (b). Incoming velocities are $v = 0$ (red, filled circles), $v = 0.02$ (blue, open circles) for (a), and $v = 0$ (red, filled circles), $v = 0.2$ (blue, open circles) for (b). Other parameters are fixed as in Figs. 6 and 10.

(nonreciprocal) behavior at $\eta = -5.8$ (see Fig. 3). The results of the interaction of the GS coming from the left and from the right with the $\mathcal{PT}$ defect are shown in Fig. 15. As one can see from Fig. 15(a), the total transmission of the GS occurs when the GS is coming from the left, while the total reflection with amplification and acceleration is observed when GS comes from the right [see Fig. 15(b)].

By placing two $\mathcal{PT}$ defects symmetrically at $x_{1,2} = \pm 20\pi$ with opposite sign of the imaginary part $\xi_{1,2} = \pm 0.02|\eta|$ we obtain that a launched GS from the left enters the intradefects

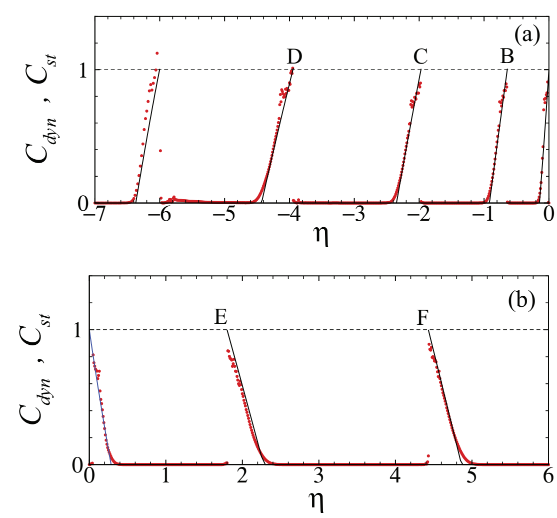

FIG. 14. (Color online) Trapping coefficient vs η corresponding to cases considered in corresponding panels of Fig. 13 The dynamical coefficient $C_{\rm dyn}$ (dotted red) refers to the case shown in Figs. 6 and 10 for $v = 0.02$, while $C_{st} = N/N_0$ corresponds to the norm of defect modes normalized to the initial norm N_0 of the incoming GS.

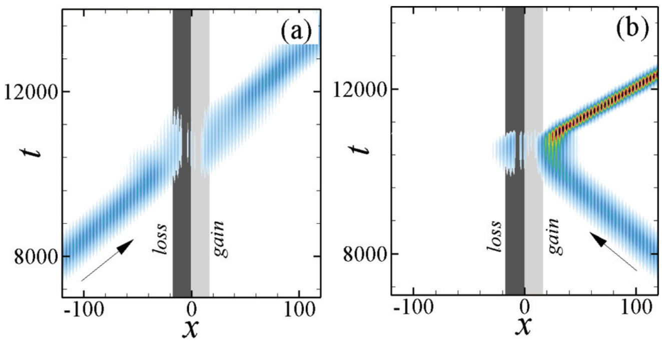

FIG. 15. (Color online) Contour plots of the GS dynamics. Defect and GS parameters: $\eta = -5.86$, $\xi/|\eta| = 0.02$, $E_s = -0.125$, $|v| = 0.05$.

region and starts to be reflected from both defects with amplification. The density plot of the dynamics is shown in Fig. 16(a) and the dynamics of the RCT coefficients are shown in Fig. 16(b).

As one can see from Fig. 16(b), the dynamics of the C coefficient has steplike behavior at each reflection in the region, between the two defects the GS are being amplified and becoming more localized, this eventually leads to the instability of the GS with emission of waves. This configuration of $\mathcal{PT}$ defects can be seen as a kind of parametric amplifier for the GS.

Similarly in Fig. 17 we have considered the case of two $\mathcal{PT}$ defects arranged with opposite facing loss sides so that a GS entering via resonant transmission into the intradefect region becomes completely depleted by the multiple reflections. One can also consider an arrangement with the facing sides of the defects having opposite signs so as to allow the storage of solitons by compensating the loss in the reflection at one side with the gain in the reflection at the other side (not shown here for brevity). $\mathcal{PT}$ defect devices based on GS will be discussed in more detail elsewhere.

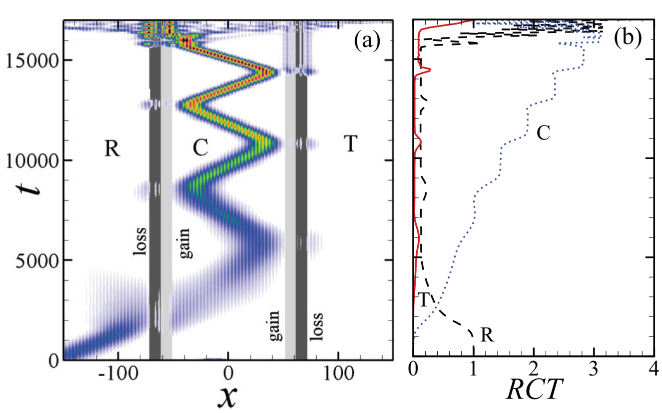

FIG. 16. (Color online) Contour plots of the GS dynamics (left panels) and time evolution of *RTC* coefficients (right panels) for a GS trapped between two adjacent $\mathcal{PT}$ defects with opposite facing gain sides and for parameter values $x_{1,2} = \pm 20\pi$, $\eta = -5.8$, $\xi_{1,2}/|\eta| = \pm 0.02$. Parameters of the initial GS are $E_s = -0.125$, $v = 0.05$. Notice the amplification of the GS at each reflection and the instability with emission of radiation which appear at later stages.

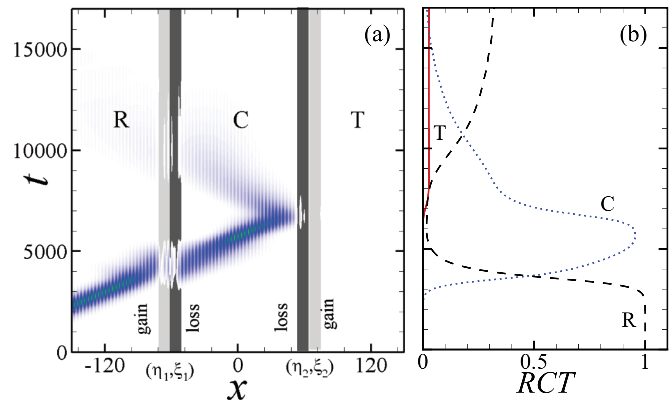

FIG. 17. (Color online) The same as in Fig. 16 with two different $\mathcal{PT}$ defects with opposite facing loss sides and for parameter values $x_{1,2} = \pm 20\pi$, $\eta_1 = -5.95$, $\xi_1/|\eta| = -0.01$ and $\eta_2 = -10$, $\xi_2/|\eta| = 0.01$. Parameters of the initial GS are $E_s = -0.125$, $v = 0.05$.

V. CONCLUSIONS

In this paper we have investigated the scattering properties of gap solitons of the periodic nonlinear Schrödinger equation (NLSE) in the presence of localized $\mathcal{PT}$-symmetric defects. The periodic potential responsible for the band-gap structure and for the existence of GSs has been taken of trigonometric form, while the localized $\mathcal{PT}$-symmetric defect was taken with the real part of the Gaussian and the imaginary part as a product of a Gaussian and a linear ramp potential (antisymmetric in space). We have shown, by means of direct numerical simulations, that by properly designing the amplitudes of real and imaginary parts of the $\mathcal{PT}$ defect it is possible to achieve a resonant transmission of the gap soliton through the defect. We showed that this phenomenon occurs for potential parameters that support localized modes inside the $\mathcal{PT}$ defect potential with the same energy and norm of the incoming soliton. The direct numerical results were found to be in good agreement with the predictions for the resonant transmission made in terms of stationary defect mode analysis, this extends previous results for conservative defects [19] to the case of $\mathcal{PT}$-symmetric defects. When the imaginary amplitude of the $\mathcal{PT}$ defect is increased we found that significant changes in the scattering properties appear. In particular, we showed the possibility of transmitted and reflected GS which gets damped or amplified during the scattering process depending on the side of the defect (loss or gain) with which the GS interacts more. We investigated this both by means of the mean imaginary part of the defect potential seen by the GS and by trajectories followed by the center of the density distribution. Scattering properties of gap solitons belonging to different band gaps and having different effective masses were also investigated. We showed that GS with effective masses of opposite sign behave similarly in $\mathcal{PT}$ defect potentials of opposite sign especially for parameter values close to high resonances. Finally, we discussed the scattering of a GS by a $\mathcal{PT}$ defect which leads to an unidirectional transmission or blockage (*diode effect*), and the amplification/depletion of a GS trapped between a pair of consecutive $\mathcal{PT}$ defects.

Finally, in closing this paper we remark that since $\mathcal{PT}$-symmetric potentials can be easily implemented in nonlinear optical systems, we expect the above results to be of experimental interest for systems such as arrays of nonlinear optical waveguides and photonic crystals.

ACKNOWLEDGMENTS

M.S. acknowledges support from the Ministero dell' Istruzione, dell' Universitá e della Ricerca (MIUR) through a *Programma di Ricerca Scientifica di Rilevante Interesse Nazionale* (PRIN)-2010 initiative. F.A. acknowledges partial support from FAPESP(Brasil).

[1] C. M. Bender and S. Boettcher, Phys. Rev. Lett. **80**, 5243 (1998).
[2] R. El-Ganainy, K. G. Makris, D. N. Christodoulides, and Z. H. Musslimani, Opt. Lett. **32**, 2632 (2007).
[3] H. Benisty *et al.*, Opt. Express **19**, 18004 (2011).
[4] J. Schindler, Z. Lin, J. M. Lee, H. Ramezani, F. M. Ellis, and T. Kottos, J. Phys. A: Math. Theor. **45**, 444029 (2012).
[5] N. Lazarides and G. P. Tsironis, Phys. Rev. Lett. **110**, 053901 (2013).
[6] K. G. Makris, R. El-Ganainy, D. N. Christodoulides, and Z. H. Musslimani, Phys. Rev. Lett. **100**, 103904 (2008).
[7] Z. Lin, H. Ramezani, T. Eichelkraut, T. Kottos, H. Cao, and D. N. Christodoulides, Phys. Rev. Lett. **106**, 213901 (2011).
[8] Z. H. Musslimani, K. G. Makris, R. El-Ganainy, and D. N. Christodoulides, Phys. Rev. Lett. **100**, 030402 (2008).
[9] F. Kh. Abdullaev, Y. V. Kartashov, V. V. Konotop, and D. A. Zezyulin, Phys. Rev. A **83**, 041805(R) (2011).
[10] A. Regensburger *et al.*, Nature (London) **488**, 167 (2012).
[11] C. Hang, G. Huang, and V. V. Konotop, Phys. Rev. Lett. **110**, 083604 (2013).
[12] M. Nazari, F. Nazari, and M. K. Moravvej-Farshi, J. Opt. Soc. Am. B **29**, 3057 (2012).
[13] S. V. Dmitriev, S. V. Suchkov, A. A. Sukhorukov, and Y. S. Kivshar, Phys. Rev. A **84**, 013833 (2011).
[14] F. Kh. Abdullaev, V. V. Konotop, M. Ogren, and M. P. Soerensen, Opt. Lett. **36**, 4566 (2011).
[15] H. Wang, W. He, L. Zheng, X. Zhu, H. Li, and Y. He, J. Phys. B: At. Mol. Opt. Phys. **45**, 245401 (2012).
[16] K. Zhou, Z. Guo, J. Wang, and S. Liu, Opt. Lett. **35**, 2928 (2010).
[17] H. Wang and J. Wang, Opt. Express **19**, 4030 (2011).
[18] S. Hu, X. Ma, D. Lu, Y. Zheng, and W. Hu, Phys. Rev. A **85**, 043826 (2012).
[19] V. A. Brazhnyi and M. Salerno, Phys. Rev. A **83**, 053616 (2011).
[20] A. Regensburger, M-A Miri, C. Bersch, J. Nager, G. Onishchukov, D. N. Christodoulides, and U. Peschel, Phys. Rev. Lett. **110**, 223902 (2013).
[21] M. Salerno, V. V. Konotop, and Yu. V. Bludov, Phys. Rev. Lett. **101**, 030405 (2008).
[22] V. V. Konotop and M. Salerno, Phys. Rev. A **65**, 021602 (2002).
[23] Z. Ahmed, Phys. Lett. A **282**, 343 (2001).
[24] A. Guo, G. J. Salamo, D. Duchesne, R. Morandotti, M. Volatier-Ravat, V. Aimez, G. A. Siviloglou, and D. N. Christodoulides, Phys. Rev. Lett. **103**, 093902 (2009).
[25] C. E. Ruter, K. G. Makris, R. EI-Ganainy, D. N. Christodoulides, M. Segev, and D. Kip, Nat. Phys. **6**, 192 (2010).
[26] S. Lepri and G. Casati, Phys. Rev. Lett. **106**, 164101 (2011); S. Lepri and B. A. Malomed, Phys. Rev. E **87**, 042903 (2013).
[27] H. Ramezani, Z. Lin, T. Kottos, and D. N. Christodoulides, Proc. SPIE 8095, Active Photonic Materials IV, 80950L (2011), doi:10.1117/12.893195.